

Discovery of a potent class I protein arginine methyltransferase fragment inhibitor

Renato Ferreira de Freitas^{1,§}, Mohammad S. Eram^{1,§}, Magdalena M. Szewczyk¹, Holger Steuber², David Smil¹, Hong Wu¹, Fengling Li¹, Guillermo Senisterra¹, Aiping Dong¹, Peter J. Brown¹, Marion Hitchcock², Dieter Moosmayer², Christian M. Stegmann², Ursula Egner², Cheryl Arrowsmith^{1,3}, Dalia Barsyte-Lovejoy¹, Masoud Vedadi^{1,4,*}, Matthieu Schapira^{1,4,*}

¹ Structural Genomics Consortium, University of Toronto, Toronto, ON M5G 1L7, Canada

² Bayer Pharma AG, Bayer Healthcare Pharmaceuticals, 13353 Berlin, Germany

³ Princess Margaret Cancer Centre and Department of Medical Biophysics, University of Toronto, Toronto, ON M5G 1L7, Canada

⁴ Department of Pharmacology and Toxicology, University of Toronto, Toronto, ON M5S 1A8, Canada

ABSTRACT

Protein methyltransferases (PMTs) are a promising target class in oncology and other disease areas. They are composed of SET domain methyltransferases, and structurally unrelated Rossmann-fold enzymes that include protein arginine methyltransferases (PRMTs). In the absence of a well-defined medicinal chemistry tool-kit focused on PMTs, most current inhibitors were identified by screening large and diverse libraries of lead-like molecules. So far, no successful fragment-based approach was reported against this target class. Here, by deconstructing potent PRMT inhibitors, we find that chemical moieties occupying the substrate arginine-binding site can act as efficient fragment inhibitors. Screening a fragment library against PRMT6 produced numerous hits, including a 300 nM inhibitor (ligand efficiency of 0.56) that decreased global histone 3 arginine 2 methylation in cells, and can serve as a warhead for the development of PRMT chemical probes.

INTRODUCTION

Protein arginine methyltransferases (PRMTs) transfer a methyl group from the cofactor S-adenosyl-L-methionine (SAM) to the terminal guanidino nitrogens of arginine on substrate proteins, and can be divided into three types (I, II, and III) according to the degree and position of methylation¹. Type I and II PRMTs convert arginine into monomethylarginine and further into asymmetric and symmetric dimethylarginine, respectively, while type III enzymes only monomethylate their substrates. In humans, PRMTs 1,3,4,6, and 8 are type I enzymes, PRMT5 and PRMT9 are type II, and PRMT7 is the only known type III PRMT. PRMT6 methylates histone H3 at R2 and histones H4/H2A at R3 *in vitro*, and is the major H3R2 methyltransferase *in vivo*. The H3R2 mark is a negative regulator of H3K4 trimethylation and transcriptional activation^{2, 3}. PRMT6 is overexpressed in various types of human cancers such as breast, bladder, lung cancers^{4, 5} or melanoma⁶, and is directly implicated in the pathogenesis of neurodegenerative diseases⁷. PRMT4 methylates Arg2, 17 and 26 of histone H3 and many non-histone proteins, including transcriptional coactivators and splicing factors, suggesting functions in transcriptional regulation and mRNA processing⁸⁻¹⁰. It has been implicated in leukemia and solid tumors¹¹⁻¹³. These results suggest that PRMT4 and PRMT6 may represent attractive therapeutic targets, and the first PRMT4 and PRMT6 chemical probes were recently reported^{14, 15}.

Although fragment-based approaches are now established as powerful tools to discover inhibitors for enzymes as well as for challenging targets (such as protein-protein interactions), there is no report of its successful application against protein

methyltransferases. In fact, chemical moieties that, in the context of large and potent inhibitors, occupy the substrate-binding site of SET domain methyltransferases are inactive as fragments against the same enzymes¹⁶. Here, we show that PRMTs can efficiently be targeted by fragment libraries, and present the first fragment inhibitor of a protein methyltransferase.

RESULTS

Fragments deconstructed from known PRMT inhibitors are efficient.

We first asked whether fragments resulting from the deconstruction of high-affinity PRMT inhibitors would still bind and retain affinity, albeit lower, toward the protein. We initially selected PRMT6 and CARM1 as model systems. Inhibitors **1** ($IC_{50} = 27$ nM) and **2** ($IC_{50} = 30$ nM) were previously reported as potent CARM1 inhibitors¹⁷ and EPZ020411 (**3**, $IC_{50} = 10$ nM) was recently disclosed as the first potent small molecule PRMT6 inhibitor¹⁵. We also find that **2b**, a close analog of **2** where the fluorine is replaced with a chlorine, is equipotent against CARM1 and PRMT6 (Supplementary Table 1). A common feature of inhibitors **1-3** is that a basic tail is anchored in the substrate arginine-binding channel of their targets (PDB codes 2Y1X, 2Y1W, 4Y30) (Figure 1)^{15, 17}. In an alternate binding mode, **2b** occupies another pocket, juxtaposed to, but distinct from the substrate binding site (PDB code 4QPP, Supplementary Table 2), but mutational analysis indicates that binding at the substrate-binding pocket mediates inhibition (data not shown). Chemical moieties occupying the substrate arginine-binding channel in the context of these potent inhibitors were tested against PRMT6 and CARM1.

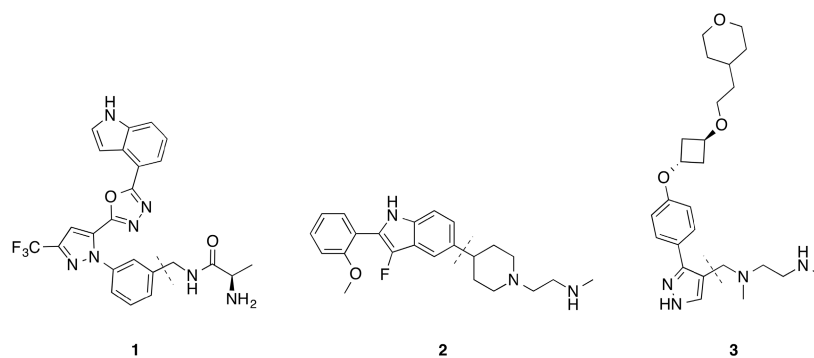


Figure 1. Structure of the inhibitors used in the deconstruction study. The alkylamino tail (right side of the dashed line) of the inhibitors was tested against CARM1 and PRMT6.

Remarkably, all three fragments (**4-6**) were active against CARM1 and PRMT6 with excellent ligand efficiency ($LE \geq 0.68$) (Table 1). In particular, the exceptionally high ligand efficiencies observed for fragments **5** and **6** are probably due to a buried electrostatic interaction between a catalytic glutamic acid (E258 in CARM1, E155 in PRMT6) and the secondary amine of the inhibitors, observed in the crystal structure of the parent compounds (PDB code 2Y1W and 4Y30). Indeed, Smith et al. have shown that electrostatic interactions define maximum efficiency of ligand binding¹⁸.

Table 1. Biochemical IC_{50} values and *in silico* characterisation of fragments derived from potent CARM1 and PRMT6 inhibitors.

Compound	Structure	CARM1 IC_{50} (μ M)	PRMT6 IC_{50} (μ M)	HA ^a	CARM1 LE ^b	PRMT6 LE	$\log D^c$
4		105 ± 7	>200	8	0.68	<0.63	-1.74
5		0.2 ± 0	2.1 ± 0.3	11	0.83	0.71	-1.61
6		3 ± 0.2	5 ± 0.6	7	1.08	1.04	-2.61

^a number of heavy atoms

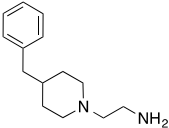
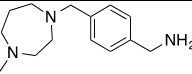
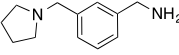
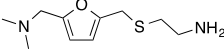
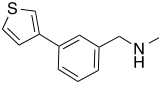
^b ligand efficiency was calculated using the equation $LE = (1.37 \times pIC_{50})/HA$; LE is expressed as kcal/mol/atom¹⁹

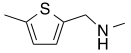
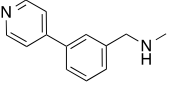
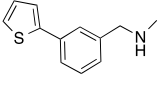
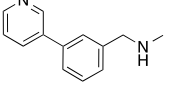
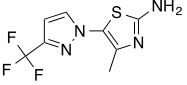
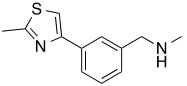
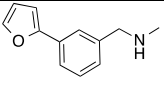
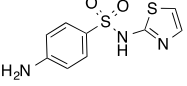
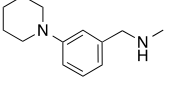
^c logD was calculated using ChemAxon's JChem for Excel, version 14.12.800.

Screening a diverse fragment library identifies PRMT6 hits.

Encouraged by the initial results from the deconstruction study, a commercial fragment library of 2040 compounds (including a pre-designed 1000-fragment set from Maybridge and 1040 fragments cherry-picked from other vendors) was screened at a concentration of 1 mM to identify inhibitors of PRMT6 and hits were re-tested in singlet at 500 μ M. Compounds with irreproducible activity, that quenched the signal, or with high Hill slopes, as well as those regarded as unattractive for further development were removed. This step eliminated 14 hits, and only 14 fragments, confirmed in triplicate, remained for further evaluation (hit rate: 0.7% - Table 2).

Table 2. Structures and Potency (IC_{50}) for fragments **7-20** Identified in the biochemical screen.

Compound	Structure	PRMT6 IC_{50} (μ M) ^a	Hill Slope	HA ^b	LE ^b	logD ^b
7		0.3 ± 0.04	1.0	16	0.56	-0.11
8		24 ± 1	1.3	17	0.37	-2.94
9		360 ± 31	1.3	14	0.34	-2.23
10		72 ± 7	1.4	14	0.41	-2.28
11		69 ± 5	1.2	14	0.41	0.73

12		99 ± 6	1.2	9	0.61	0.27
13		100 ± 18	1.1	15	0.37	-0.27
14		125 ± 23	1.2	14	0.38	0.76
15		104 ± 9	1.1	15	0.36	-0.26
16		46 ± 5	1.0	16	0.37	2.13
17		136 ± 24	1.1	15	0.35	0.17
18		146 ± 13	1.1	14	0.38	0.08
19		430 ± 34	1.2	16	0.29	0.45
20		170 ± 8	1.2	15	0.34	0.29

^a mean ± standard deviation derived from triplicate experiments

^b as in Table 1

The fragment screen provided an array of hits with reasonable potency ($IC_{50} = 0.3 - 430 \mu\text{M}$) and ligand efficiencies ($LE \geq 0.29$). A common feature shared by most of the 14 fragments is the presence of two rings with an alkylamine side chain attached to the central ring. Fragment **7** (MW = 218.3 Da) showed a submicromolar IC_{50} ($0.3 \pm 0.04 \mu\text{M}$) against PRMT6 and excellent ligand efficiency ($LE = 0.56$). The binding of this fragment was further confirmed by isothermal titration calorimetry (ITC), revealing a dissociation constant (K_D) of $0.97 \mu\text{M}$ (Figure 2a). The ITC experiment also provided the thermodynamic signature of **7** binding to PRMT6 (Figure 2b), characterized by a favorable change in enthalpy ($\Delta H = -17.2 \text{ kcal/mol}$) and a large, unfavorable entropic

component ($-T\Delta S = 9.0$ kcal/mol) due to loss of translational and rotational movement of the unbound fragment²⁰. This profile is consistent with binding being driven by enthalpy, indicating the formation of strong hydrogen bonds and hydrophobic interactions with the pocket.

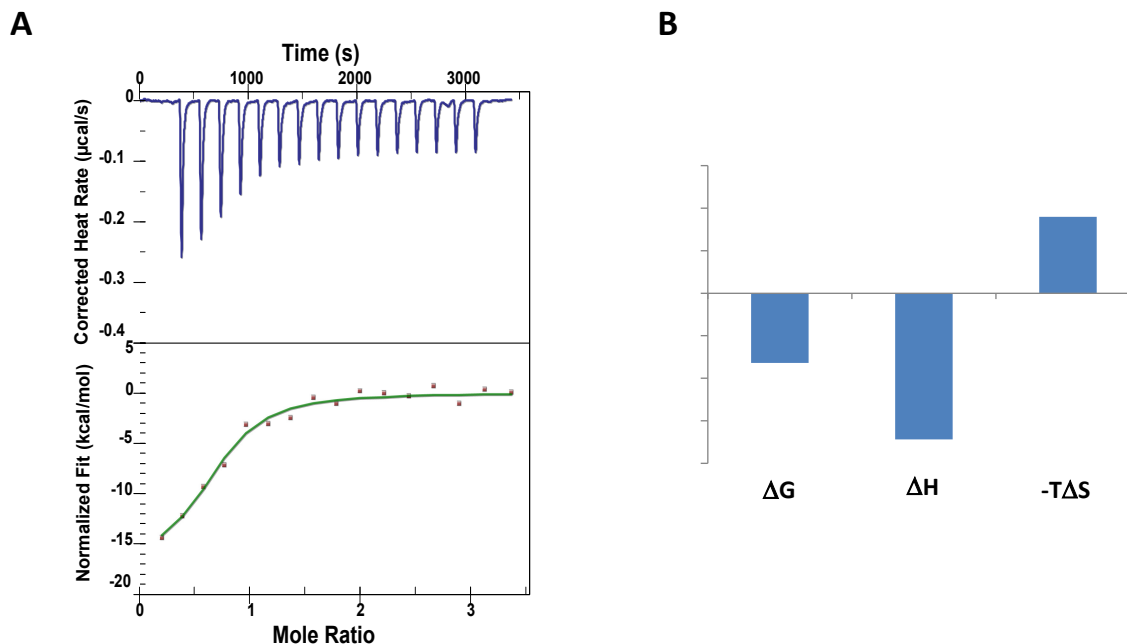


Figure 2. a) Isothermal titration calorimetry data showing the titration of fragment **7** into PRMT6 (top) and fit curve (bottom). b) Thermodynamic signatures of the PRMT6-7 complex, with Gibbs free energy of binding (ΔG), enthalpy (ΔH) and entropy ($-T\Delta S$).

We next determined the selectivity profile of **7** against a panel of 30 human methyltransferases (Figure 3). With the exception of Type I PRMTs (Table 3, Supplementary Figure 1), no significant inhibition was observed for all other methyltransferases tested up to 50 μM . Significant inhibitory activity was observed on CARM1 ($\text{IC}_{50} = 1$ μM) and PRMT8 ($\text{IC}_{50} = 2.1$ μM). Considering the size of **7**, this

selectivity profile is relatively narrow, and suggests that this fragment represents a good template for further optimization.

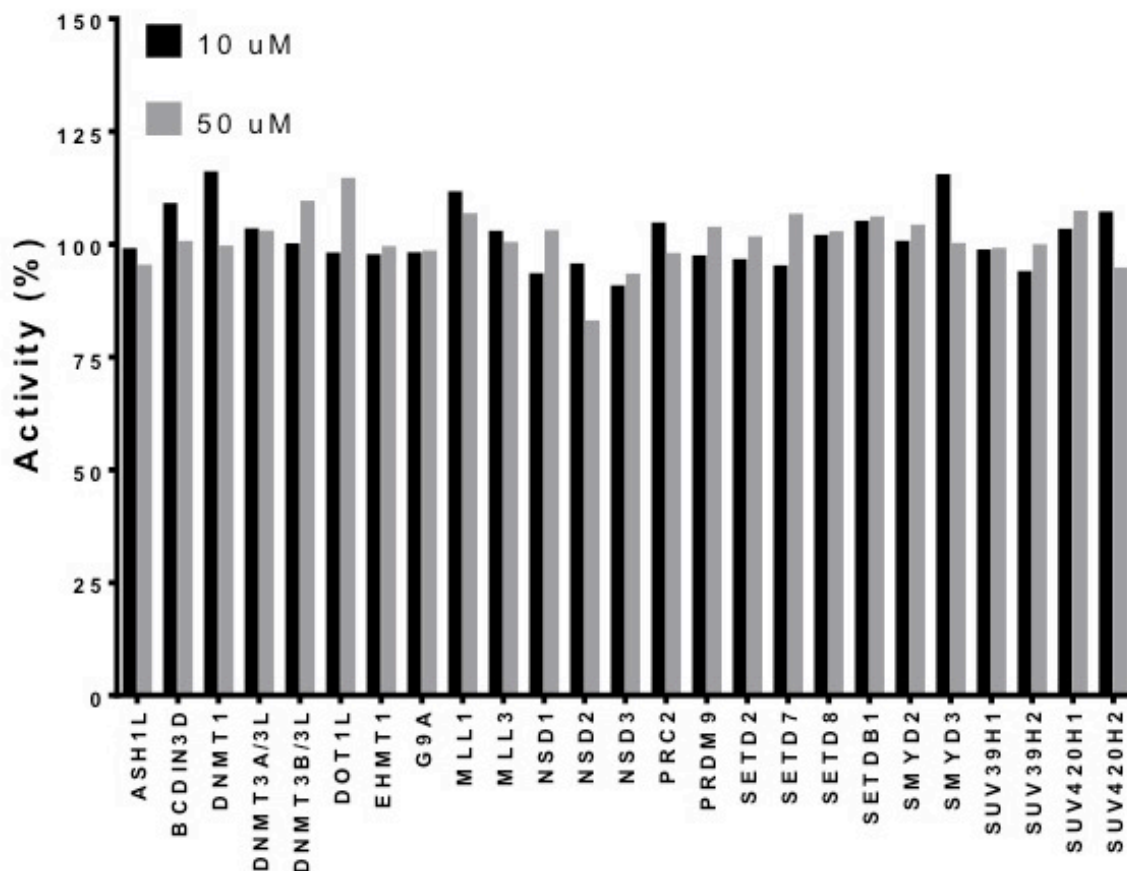


Figure 3: Selectivity profile of fragment 7 against a panel of 25 human methyltransferases

Table 3: IC₅₀ determination for fragments 4, 5, 6, and 7 on PRMTs

Target	Fragment 4		Fragment 5		Fragment 6		Fragment 7	
	IC ₅₀ (μM)	Hill Slope	IC ₅₀ (μM)	Hill Slope	IC ₅₀ (μM)	Hill Slope	IC ₅₀ (μM)	Hill Slope
PRMT1	>1000	NA	48 ± 7	2.1	39 ± 3	1.4	12 ± 0.6	1.7
PRMT3	>1000	NA	>500	NA	35 ± 2	1.4	19 ± 1	2.2
PRMT4	105 ± 7	0.7	0.2 ± 0	0.5	3 ± 0.2	0.8	1 ± 0.04	0.7

PRMT5	NI	NA	NI	NA	NI	NA	NI	NA
PRMT6	>200	NA	2.1 ± 0.3	0.8	5 ± 0.6	1	0.3 ± 0.04	0.8
PRMT7	NI	NA	NI	NA	NI	NA	NI	NA
PRMT8	>200	NA	15 ± 1	0.7	7 ± 1.2	1	2.1 ± 0.2	0.7

Fragment 7 competes with the substrate arginine.

To verify that fragment 7 occupies the Rme binding channel of PRMT6, we solved the crystal structure of the PRMT6-fragment 7 complex (Figure 4, Supplementary Table 3). The alkylamino side-chain is deeply buried in the substrate arginine pocket. The amine groups make direct and water-mediated hydrogen bonds with E155, E164, and H317. The superposition of 7, 2 and 3 in complex with PRMT6, CARM1 and PRMT6 respectively reveals that the alkylamino side chain of 7 align almost perfectly with bound conformation of inhibitors 2 and 3 (Supplementary Figure 2). A large hydrophobic shelf at residues L46, Y47, C50, and Y51 of PRMT6 is available immediately next to the bound fragment and can be exploited to increase potency and selectivity (Figure 4, Supplementary Figure 3). A leucine-rich pocket neighboring the substrate-binding site, lined by leucines 162,167,171, 267 and 353 is also partially occupied by 7 (2 PRMT6 chains occupied out of 4 in the crystal unit cell - Figure 4B, Supplementary Figure 4).

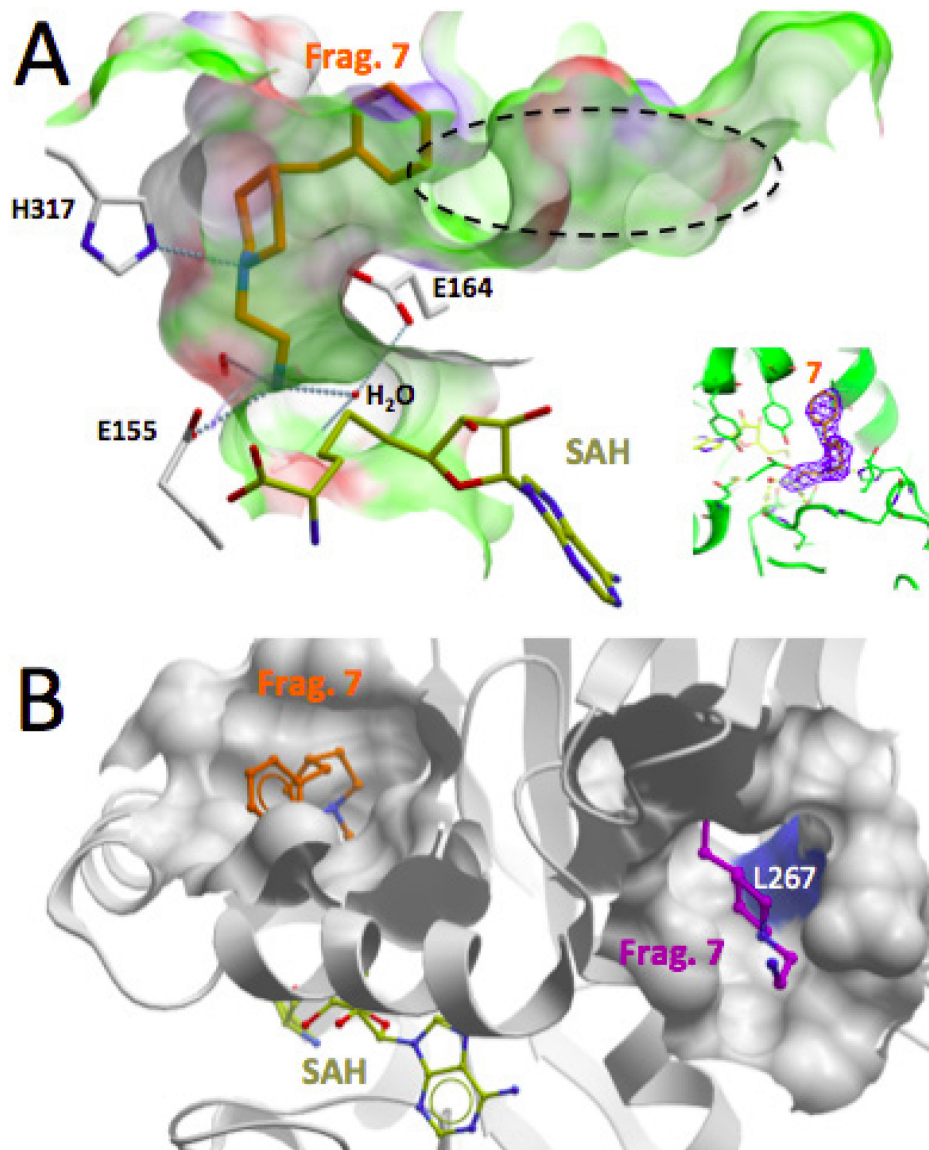


Figure 4. A) Fragment 7 (orange) occupies the substrate arginine binding site of PRMT6. The nitrogens of the alkylamino tail make hydrogen bonds (blue dotted lines) with surrounding residues. A hydrophobic shelf (dashed oval) is available for fragment expansion. Insert: Omit $F_o - F_c$ electron-density of the crystallized fragment shown at 3σ . B) 7 (magenta) occupies a second binding pocket in two out of four PRMT6 subunits present in the asymmetric unit. The cofactor product, S-adenosyl-homocysteine (SAH), is shown in yellow.

The selectivity of fragment **7** against PMRT1 (30 fold) and PRMT3 (47.5 fold) was not expected given the high sequence similarity of the arginine pocket among these enzymes. Three residues in the vicinity of **7** are not conserved between PRMT6 and the other two PRMTs: C50 (serine in PRMT1 and 3), V56 (isoleucine in PRMT1 and 3) and H163 (tyrosine in PRMT1 and phenylalanine in PRMT3). These residues are at the mouth of the arginine-binding pocket, and the first two are in direct contact with the aromatic ring of **7**. Structural alignment of the PRMT6 complex structure with PRMT3 (PDB code 1F3L) does not clearly rationalize the observed selectivity (Supplementary Figure 5). A minor steric clash between **7** and I226 of PRMT3 (I51 in PRMT1, V56 in PRMT6) could be responsible for the reduced activity on PRMT1 and PRMT3.

To characterize the mechanism of action of **7** in solution, IC_{50} values were determined at various concentrations of SAM and peptide substrate (Figure 5A,B). Increasing concentration of substrate peptide or cofactor did not affect IC_{50} values, indicative of a non-competitive inhibitory mechanism. A similar result was obtained for the potent PRMT6 inhibitor EPZ020411 (compound **3**) (Supplementary Figure 6), which was also found to occupy the substrate-binding site by X-ray crystallography¹⁵. Two interpretations are possible. PRMT6 inhibition is mediated via binding of **7** at an allosteric site, such as the one that is partially occupied by the fragment in the crystal structure (Figure 4B). Alternatively, binding at the substrate arginine-binding pocket, which is fully occupied by **7** in the crystal, mediates inhibition, but the substrate peptide is making additional interactions with PRMT6 outside of the catalytic site, and is not efficiently displaced from PRMT6 by the fragment (a similar argument was proposed for a substrate competitor of SMYD3²¹). To determine which is the correct interpretation, we

tested the inhibitory activity of **7** on a PRMT6 construct where L267, a residue lining the allosteric site (as shown in Figure 4), is mutated to a glutamic acid. We find that mutation at the allosteric site has no significant effect on the inhibitory activity of **7** (IC_{50} value of $0.23 \pm 0.02 \mu\text{M}$ and $0.39 \pm 0.01 \mu\text{M}$ against wild type and mutant PRMT6 respectively) (Figure 5C,D), supporting the idea that binding of **7** at the catalytic site drives PRMT6 inhibition.

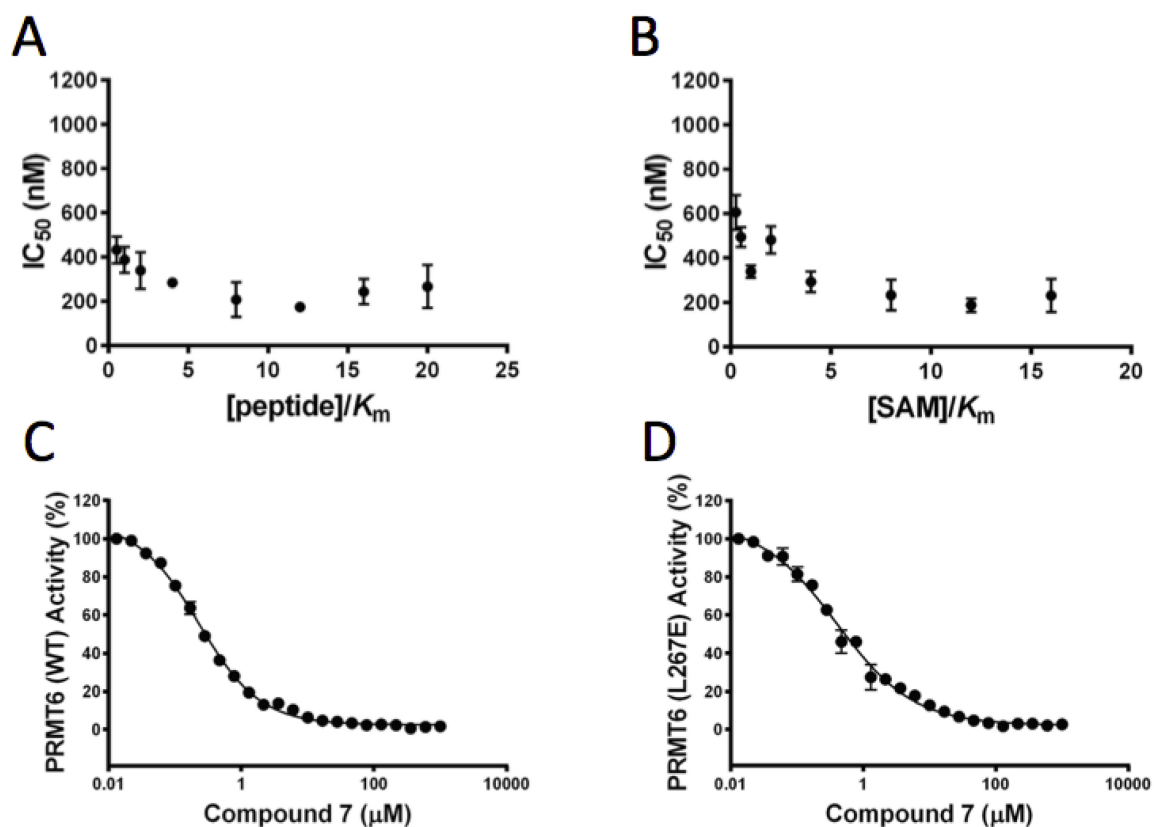


Figure 5. Mechanism of action (MOA) of fragment **7**. Possible competition of **7** with (A) peptide and (B) SAM was assessed by determining the IC_{50} values at various concentrations of one substrate and keeping the second substrate at saturation (A; SAM at 12 μM , B; peptide at 2.5 μM). The error bars represent the standard deviation of three sets of experiments. (C,D) Dose-dependent inhibition of wild-type or L267E PRMT6 by

fragment **7** resulted in IC₅₀ values of $0.23 \pm 0.02 \mu\text{M}$ (Hill Slope of 0.9) and $0.39 \pm 0.01 \mu\text{M}$ (Hill Slope of 0.7) respectively.

Fragment 7 is active in cells. PRMT6 is believed to control the global level of asymmetrically dimethylated H3R2 (H3R2me2a)³. Since knock-down of PRMT6 resulted only in small reduction of H3R2me2a after 4 days (probably due to slow turnover, data not shown), we used an overexpression system to test the effect of **7**. HEK293 cells were transfected with PRMT6 or its catalytically dead mutant (V86K/D88A) and treated with **7** for 20 h. The fragment was able to inhibit the methylation of H3R2 in a dose dependent manner, with an IC₅₀ of $21 \pm 3 \mu\text{M}$ (Figure 6). We did not observe any cytotoxic effect of the inhibitor within this time frame at any tested concentration. Although weak, this is an encouraging result considering that fragment **7** is rather hydrophilic ($\log D_{\text{calc}} = -0.11$). To achieve good membrane permeation, a logD value of >0.5 is required for compounds with a molecular weight of $<300 \text{ Da}$ ²². With a molecular weight of only 218.3 Da and 16 heavy atoms, there is room to optimize the permeability of this fragment, along with enzymatic and cellular activity, by adding hydrophobic groups while avoiding violation of the drug-like chemical space²³.

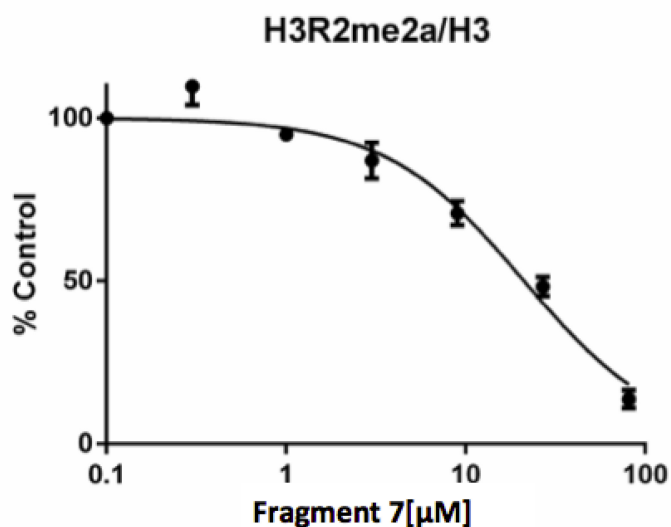
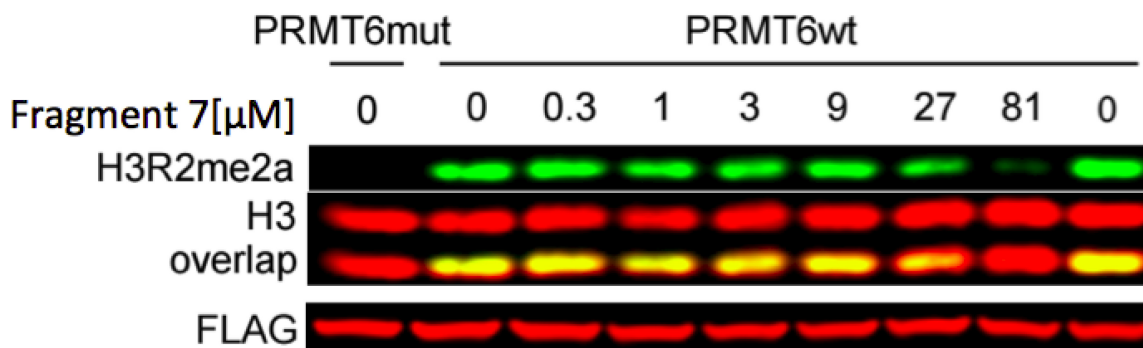


Figure 6. Fragment 7 inhibits in a dose-dependent manner the methylation of H3R2 in 293 cells transfected with PRMT6 ($IC_{50} = 21 \pm 3 \mu\text{M}$). HEK293 cells were transfected with FLAG-tagged PRMT6 or its catalytically dead mutant V86K/D88A (PRMT6mut) and treated with inhibitor for 20 h. H3R2me2a levels were determined by Western blot. The graph represents a nonlinear fit of H3R2me2a signal intensity normalized to total histone H3. The results are MEAN \pm SEM of 3 replicates.

CONCLUSION

We previously found that fragments occupying the Kme binding channel of SET domain methyltransferases are poor inhibitors¹⁶. In striking contrast, we now show that fragments

occupying the Rme binding channel of PRMTs are efficient inhibitors and that PRMTs are amenable to fragment screening. We speculate that this surprising result is due to the fact that SET domain PMTs and PRMTs - which are Rossmann fold enzymes - have entirely different structures^{24, 25}. Difference in structural plasticity of the binding pocket cannot be invoked to explain this contrasting result: the substrate lysine sites of G9a and SMYD2 are already preformed in cofactor-bound structures (PDB code 2O8J and 3RIB respectively), and yet fragments are inactive. Conversely, the substrate site of PRMT6 is properly, but incompletely formed in the cofactor-bound structure, yet fragments can bind with high efficiency. We rather propose that the presence of a conserved catalytic glutamic acid at the bottom of the arginine binding pockets of PRMTs constitutes a strong interaction hotspot that can efficiently interact with positively charged fragments, while no equivalent exists in the lysine binding pocket of SET domain enzymes.

The results presented here support a strategy to develop novel Class I PRMT inhibitors: the Rme binding channel is conserved across Class I PRMTs²⁵, and **7** as well as other fragments shown in Table 1 may serve as warheads for Class I PRMT inhibition. The juxtaposed hydrophobic shelf (which is occupied by a potent PRMT6 inhibitor reported recently¹⁵) is structurally diverse²⁵ and can be exploited to access inhibitors with distinct selectivity profiles.

EXPERIMENTAL SECTION

Chemistry

All compounds tested in vitro were >95% pure. Purity determination was conducted by UV absorbance at 254 nm during tandem liquid chromatography/mass spectrometry (LCMS) using a Waters Acquity separations module. Identity was determined via low-resolution mass spectrometry (LRMS) conducted in positive ion mode using a Waters Acquity SQD mass spectrometer (electrospray ionization source) fitted with a PDA detector. Mobile phase A consisted of 0.1% formic acid in water, while mobile phase B consisted of 0.1% formic acid in acetonitrile. The gradient ran from 5% to 95% mobile phase B over 3 minutes at 0.5 mL/min. An Acquity CSH C18 (2.1 x 50 mm, 130 Å, 1.7 µm) column (Part No. 186005296) was used with column temperature maintained at 25 °C. The sample solution injection volume was 5 µL. Compounds 2b and 3 were synthesized as previously described^{15, 26}. String formulas of all compounds are provided in Supplementary Table 4.

Biochemical activity assays

Scintillation proximity assay (SPA) was exploited for the initial screening and IC₅₀ determination were performed as described before²⁷. In brief, transfer of the labeled methyl group from tritiated S-adenosylmethionine (³H-SAM, PerkinElmer Life Sciences) to peptide substrate was monitored by capturing the biotinylated peptide after enzymatic reaction in streptavidin / scintillant-coated microplate (FlashPlate® PLUS; PerkinElmer Life Sciences) and measuring Luminescence using a TopCount NXT™ Microplate Scintillation and Luminescence Counter (PerkinElmer Life Sciences). The reaction mixture (20 µL in volume) contained 20 mM Bis-Tris-Propane (BTP, pH 7.5); 0.01% Tween-20 and 10 mM DTT; 50 nM PRMT6; 2.3 µM SAM and 0.6 µM peptide substrate. The C-terminally biotinylated peptide composed

of the first 24 residues of histone H4 (SGRGKGGKGLGKGGAKRHRKVLRLDK-Biotin) was used as substrate. The screening and IC₅₀ determination experiments were carried out under balanced conditions at K_m concentration of both substrate and cofactor.

Fragment library screening

The reduced complexity fragment library of 2040 compounds was screened at 1 mM of compounds using SPA assay. The hits from the initial screen were cherry picked and confirmed by repeating the assay at 500 μ M final compound concentrations. All hits were tested for possible signal quenching effect.

Mechanism of action determination

The mechanism of action of the fragment **7** was determined biochemically using the method described previously²⁸. In brief, to assess the competition with peptide, the SAM concentration was kept at saturation and IC₅₀ values were determined at different peptide concentrations (0.5, 1, 2, 4, 8, 12, 16, and 20 \times K_m). To assess the competition of the compound with SAM the peptide concentration was kept at saturation and the potency of the compound was assessed at various SAM concentrations (0.25, 0.5, 1, 2, 4, 8, 12, and 16 \times K_m).

Isothermal titration calorimetry

Isothermal titration calorimetry (ITC) was performed at 25°C in a Nano ITC instrument (TA Instruments, USA). The cell was loaded with 33 μ M PRMT6 and 3.3% DMSO in PBS buffer. The syringe was loaded with 100 μ M fragment **7** and 3.3% DMSO in PBS. 2 μ L volumes were injected at 180 seconds intervals (25

injections in total). The data were analyzed using “Nano Analyze” software supplied by the instrument manufacturer and fit to a one binding site independent model.

Methyltransferase selectivity profiling

The selectivity of the fragment 7 was determined against a panel of 30 lysine, arginine, and DNA methyltransferases^{27, 29-31} at two compound concentrations of 10 and 50 μ M.

Cloning, expression and purification

DNA fragment encoding human PRMT6 was cloned into a baculovirus expression vector pFBOH-MHL (http://www.thesgc.org/sites/default/files/toronto_vectors/pFBOH-MHL.pdf). The protein was expressed in Sf9 cells as an N-terminal hexa-His tag fusion protein. The harvested cells were resuspended in lysis buffer containing 20 mM Tris-HCl, pH 8.0, 500 mM NaCl, 5 mM imidazol, 2 mM β -mercaptoethanol, 5% glycerol, 0.6% NP-40, protease inhibitor cocktail (Roche), 3000 U of benzonase (Novagen). Cells were lysed by brief sonication. The clarified lysate was loaded onto a 2-mL TALON column (Clontech). The column was washed with 50 column volumes of 20 mM Tris-HCl buffer, pH 8.0, containing 500 mM NaCl, 5% glycerol and 5 mM imidazole. The bound protein was eluted with elution buffer containing 20 mM Tris-HCl, pH 8.0, 500 mM NaCl, 5% glycerol, 250 mM imidazole. The eluted protein was further purified to homogeneity on a Superdex200 column (GE Healthcare), equilibrated with 20 mM Tris-HCl buffer, pH 8.0, and 150 mM NaCl. Pooled fractions containing PRMT6 were subjected to TEV treatment to remove His-tag. The protein was further purified to homogeneity by ion-exchange chromatography.

X-ray crystallography

Cocrystallization of PRMT6 in complex with **7** was carried out using a protein solution at 10 mg/ml in presence of 2 mM SAH, 3 mM of compound **7** (dissolved from a previously prepared 100 mM DMSO stock solution), followed by mixing 1 μ L of the protein solution with 1 μ L of the reservoir solution containing 25 % PEG 1500, 0.1 M MMT, pH 8. X-ray diffraction data for the PRMT6-**7** complex were collected at Bessy II, Berlin, Germany³². Data were processed using XDS³³ as implemented in XDSAPP³⁴, model building and refinement was carried out using COOT³⁵ and REFMAC³⁶.

Cellular activity assay

Hek293 cells were grown in 12-well plates in DMEM supplemented with 10% FBS, penicillin (100 units/ml) and streptomycin (100 μ g/ml). 50 % confluent cells were transfected with FLAG-tagged PRMT6/mutant V86K, D88A PRMT6 (1 μ g of DNA per well) using jetPRIME® transfection reagent (Polyplus-Transfection), following manufacturer instructions. After 4 h media were removed and cells were treated with compound **7** at indicated concentrations or DMSO control. After 20 h media was removed and cells were lysed in 100 μ l of total lysis buffer (in mM: 20 Tris-Hcl pH=8, 150 NaCl, 1 EDTA, 10 MgCl₂, 0.5% Triton-X100, 12.5 U/ml benzonase (Sigma), complete EDTA-free protease inhibitor cocktail (Roche)). After 3 min. incubation at RT, SDS was added to final 1% concentration. Total cell lysates were resolved in 4-12% Bis-Tris Protein Gels (Invitrogen) with MOPS buffer (Invitrogen) and transferred in for 1.5h (80 V) onto PVDF membrane (Millipore) in Tris-Glycine transfer buffer containing 20% MeOH and 0.05% SDS. Blots were blocked for 1h in

blocking buffer (5% milk in 0.1% Tween 20 PBS) and incubated with primary antibodies: mouse anti-H3 (1:1000, Abcam #10799), rabbit anti-H3R2me2a (1:1000, Millipore, 04-808), mouse anti-FLAG (1:5000, Sigma #F1804) in blocking buffer o/n at 4°C. After five washes with 0.1% Tween 20 PBS the blots were incubated with goat-anti rabbit (IR800 conjugated, LiCor #926-32211) and donkey anti-mouse (IR 680, LiCor #926-68072) antibodies (1:5000) in Odyssey Blocking Buffer (LiCor) for 1h at RT and washed five times with 0.1% Tween 20 PBS. The signal was read on an Odyssey scanner (LiCor) at 800 nm and 700 nm.

ASSOCIATED CONTENT

Supporting Information

The Supporting Information is available free of charge on the ACS Publications website.

Biochemical selectivity profile of compound **2b**, structure factors of PRMT6 in complex with compound **2b** and fragment **7**, dose response curves of Type I PRMTs to inhibition by compounds **4** to **7**, superimposed structures of **7** complexed to PRMT6 with **2** and **3** complexed with CARM1

Accession Codes

PRMT6 in complex with fragment 7: 5EGS. PRMT6 in complex with compound 2b: 4QPP

AUTHOR INFORMATION

Corresponding Authors

*Email: masoud.vedadi@utoronto.ca, matthieu.schapira@utoronto.ca

Notes

\$ These authors contributed equally to this work

H.S., C.S., D.M., M.H. and U.E are employed by Bayer Pharma AG and may own stock of Bayer AG. This does not alter these authors' adherence to J.Med. Chem.'s policies on sharing data and materials.

All other authors declare no competing financial interest

ACKNOWLEDGEMENTS

The SGC is a registered charity (number 1097737) that receives funds from AbbVie, Bayer Pharma AG, Boehringer Ingelheim, Canada Foundation for Innovation, Eshelman Institute for Innovation, Genome Canada, Innovative Medicines Initiative (EU/EFPIA) [ULTRA-DD grant no. 115766], Janssen, Merck & Co., Novartis Pharma AG, Ontario Ministry of Economic Development and Innovation, Pfizer, São Paulo Research Foundation-FAPESP, Takeda, and the Wellcome Trust. Tina Stromeyer and Anne Sparmann are acknowledged for excellent technical support.

ABBREVIATIONS USED

PMT, protein methyltransferases; PRMT, Protein arginine methyltransferases; SAM, S-adenosyl-L-methionine; SAH, S-adenosyl-homocysteine

REFERENCES

1. Bedford, M. T.; Richard, S. Arginine methylation an emerging regulator of protein function. *Mol Cell* **2005**, 18, 263-72.

2. Hyllus, D.; Stein, C.; Schnabel, K.; Schiltz, E.; Imhof, A.; Dou, Y.; Hsieh, J.; Bauer, U. M. PRMT6-mediated methylation of R2 in histone H3 antagonizes H3 K4 trimethylation. *Genes Dev* **2007**, *21*, 3369-80.
3. Guccione, E.; Bassi, C.; Casadio, F.; Martinato, F.; Cesaroni, M.; Schuchlantz, H.; Luscher, B.; Amati, B. Methylation of histone H3R2 by PRMT6 and H3K4 by an MLL complex are mutually exclusive. *Nature* **2007**, *449*, 933-7.
4. Phalke, S.; Mzoughi, S.; Bezzi, M.; Jennifer, N.; Mok, W. C.; Low, D. H.; Thike, A. A.; Kuznetsov, V. A.; Tan, P. H.; Voorhoeve, P. M.; Guccione, E. p53-Independent regulation of p21Waf1/Cip1 expression and senescence by PRMT6. *Nucleic Acids Res* **2012**, *40*, 9534-42.
5. Yoshimatsu, M.; Toyokawa, G.; Hayami, S.; Unoki, M.; Tsunoda, T.; Field, H. I.; Kelly, J. D.; Neal, D. E.; Maehara, Y.; Ponder, B. A.; Nakamura, Y.; Hamamoto, R. Dysregulation of PRMT1 and PRMT6, Type I arginine methyltransferases, is involved in various types of human cancers. *Int J Cancer* **2011**, *128*, 562-73.
6. Limm, K.; Ott, C.; Wallner, S.; Mueller, D. W.; Oefner, P.; Hellerbrand, C.; Bosserhoff, A. K. Deregulation of protein methylation in melanoma. *Eur J Cancer* **2013**, *49*, 1305-13.
7. Scaramuzzino, C.; Casci, I.; Parodi, S.; Lievens, P. M.; Polanco, M. J.; Milioto, C.; Chivet, M.; Monaghan, J.; Mishra, A.; Badders, N.; Aggarwal, T.; Grunseich, C.; Sambataro, F.; Basso, M.; Fackelmayer, F. O.; Taylor, J. P.; Pandey, U. B.; Pennuto, M. Protein arginine methyltransferase 6 enhances polyglutamine-expanded androgen receptor function and toxicity in spinal and bulbar muscular atrophy. *Neuron* **2015**, *85*, 88-100.
8. Yang, Y.; Bedford, M. T. Protein arginine methyltransferases and cancer. *Nat Rev Cancer* **2013**, *13*, 37-50.
9. Cheng, D.; Cote, J.; Shaaban, S.; Bedford, M. T. The arginine methyltransferase CARM1 regulates the coupling of transcription and mRNA processing. *Mol Cell* **2007**, *25*, 71-83.
10. Lee, Y. H.; Coonrod, S. A.; Kraus, W. L.; Jelinek, M. A.; Stallcup, M. R. Regulation of coactivator complex assembly and function by protein arginine methylation and demethylination. *Proc Natl Acad Sci U S A* **2005**, *102*, 3611-6.
11. Vu, L. P.; Perna, F.; Wang, L.; Voza, F.; Figueroa, M. E.; Tempst, P.; Erdjument-Bromage, H.; Gao, R.; Chen, S.; Paietta, E.; Deblasio, T.; Melnick, A.; Liu, Y.; Zhao, X.; Nimer, S. D. PRMT4 blocks myeloid differentiation by assembling a methyl-RUNX1-dependent repressor complex. *Cell Rep* **2013**, *5*, 1625-38.
12. Ou, C. Y.; LaBonte, M. J.; Manegold, P. C.; So, A. Y.; Ianculescu, I.; Gerke, D. S.; Yamamoto, K. R.; Ladner, R. D.; Kahn, M.; Kim, J. H.; Stallcup, M. R. A coactivator role of CARM1 in the dysregulation of beta-catenin activity in colorectal cancer cell growth and gene expression. *Mol Cancer Res* **2011**, *9*, 660-70.
13. Frietze, S.; Lupien, M.; Silver, P. A.; Brown, M. CARM1 regulates estrogen-stimulated breast cancer growth through up-regulation of E2F1. *Cancer Res* **2008**, *68*, 301-6.
14. Eram, M. S.; Shen, Y.; Szewczyk, M. M.; Wu, H.; Senisterra, G.; Li, F.; Butler, K. V.; Kaniskan, H. U.; Speed, B. A.; Dela Sena, C.; Dong, A.; Zeng, H.; Schapira, M.; Brown, P. J.; Arrowsmith, C. H.; Barsyte-Lovejoy, D.; Liu, J.; Vedadi, M.; Jin, J. A Potent,

Selective, and Cell-Active Inhibitor of Human Type I Protein Arginine Methyltransferases. *ACS Chem Biol* **2015**.

15. Mitchell, L. H.; Drew, A. E.; Ribich, S. A.; Rioux, N.; Swinger, K. K.; Jacques, S. L.; Lingaraj, T.; Boriack-Sjodin, P. A.; Waters, N. J.; Wigle, T. J.; Moradei, O.; Jin, L.; Riera, T.; Porter-Scott, M.; Moyer, M. P.; Smith, J. J.; Chesworth, R.; Copeland, R. A. Aryl Pyrazoles as Potent Inhibitors of Arginine Methyltransferases: Identification of the First PRMT6 Tool Compound. *ACS Med Chem Lett* **2015**, 6, 655-9.

16. Nguyen, K. T.; Li, F.; Poda, G.; Smil, D.; Vedadi, M.; Schapira, M. Strategy to target the substrate binding site of SET domain protein methyltransferases. *J Chem Inf Model* **2013**, 53, 681-91.

17. Sack, J. S.; Thieffine, S.; Bandiera, T.; Fasolini, M.; Duke, G. J.; Jayaraman, L.; Kish, K. F.; Klei, H. E.; Purandare, A. V.; Rosettani, P.; Troiani, S.; Xie, D.; Bertrand, J. A. Structural basis for CARM1 inhibition by indole and pyrazole inhibitors. *Biochem J* **2011**, 436, 331-9.

18. Smith, R. D.; Engdahl, A. L.; Dunbar, J. B., Jr.; Carlson, H. A. Biophysical limits of protein-ligand binding. *J Chem Inf Model* **2012**, 52, 2098-106.

19. Hopkins, A. L.; Keseru, G. M.; Leeson, P. D.; Rees, D. C.; Reynolds, C. H. The role of ligand efficiency metrics in drug discovery. *Nat Rev Drug Discov* **2014**, 13, 105-21.

20. Murray, C. W.; Verdonk, M. L. The consequences of translational and rotational entropy lost by small molecules on binding to proteins. *J Comput Aided Mol Des* **2002**, 16, 741-53.

21. Mitchell, L. H.; Boriack-Sjodin, P. A.; Smith, S.; Thomenius, M.; Rioux, N.; Munchhof, M.; Waters, N. J.; Wigle, T. J.; Scott, W. G.; Copeland, R. A.; Smith, J. J.; Chesworth, R. Novel oxindole sulfonamides and sulfamides: EPZ031686 the first orally bioavailable small molecule SMYD3 inhibitor. *ACS Med Chem Lett* **2015**, 1.

22. Waring, M. J. Defining optimum lipophilicity and molecular weight ranges for drug candidates-Molecular weight dependent lower logD limits based on permeability. *Bioorg Med Chem Lett* **2009**, 19, 2844-51.

23. Lipinski, C. A.; Lombardo, F.; Dominy, B. W.; Feeney, P. J. Experimental and computational approaches to estimate solubility and permeability in drug discovery and development settings. *Adv Drug Deliv Rev* **2001**, 46, 3-26.

24. Schapira, M. Structural Chemistry of Human SET Domain Protein Methyltransferases. *Curr Chem Genomics* **2011**, 5, 85-94.

25. Schapira, M.; Ferreira de Freitas, R. Structural biology and chemistry of protein arginine methyltransferases. *Med. Chem. Commun.* **2014**, 5, 1779-1788.

26. Purundare, A. V.; Wan, H.; Huynh, T. N. Heterocyclic inhibitors of protein arginine methyl transferases. *Patent US 2006/0235037* **2006**.

27. Eram, M. S.; Bustos, S. P.; Lima-Fernandes, E.; Siarheyeva, A.; Senisterra, G.; Hajian, T.; Chau, I.; Duan, S.; Wu, H.; Dombrovski, L.; Schapira, M.; Arrowsmith, C. H.; Vedadi, M. Trimethylation of histone H3 lysine 36 by human methyltransferase PRDM9 protein. *J Biol Chem* **2014**, 289, 12177-88.

28. Smil, D.; Eram, M. S.; Li, F.; Kennedy, S.; Szewczyk, M. M.; Brown, P. J.; Barsyte-Lovejoy, D.; Arrowsmith, C. H.; Vedadi, M.; Schapira, M. Discovery of a Dual PRMT5-PRMT7 Inhibitor. *ACS Med Chem Lett* **2015**, 6, 408-12.

29. Allali-Hassani, A.; Kuznetsova, E.; Hajian, T.; Wu, H.; Dombrovski, L.; Li, Y.; Graslund, S.; Arrowsmith, C. H.; Schapira, M.; Vedadi, M. A Basic Post-SET Extension

of NSDs Is Essential for Nucleosome Binding In Vitro. *J Biomol Screen* **2014**, 19, 928-935.

30. Barsyte-Lovejoy, D.; Li, F.; Oudhoff, M. J.; Tatlock, J. H.; Dong, A.; Zeng, H.; Wu, H.; Freeman, S. A.; Schapira, M.; Senisterra, G. A.; Kuznetsova, E.; Marcellus, R.; Allali-Hassani, A.; Kennedy, S.; Lambert, J. P.; Couzens, A. L.; Aman, A.; Gingras, A. C.; Al-Awar, R.; Fish, P. V.; Gerstenberger, B. S.; Roberts, L.; Benn, C. L.; Grimley, R. L.; Braam, M. J.; Rossi, F. M.; Sudol, M.; Brown, P. J.; Bunnage, M. E.; Owen, D. R.; Zaph, C.; Vedadi, M.; Arrowsmith, C. H. (R)-PFI-2 is a potent and selective inhibitor of SETD7 methyltransferase activity in cells. *Proc Natl Acad Sci U S A* **2014**, 111, 12853-8.

31. Eram, M. S.; Kuznetsova, E.; Li, F.; Lima-Fernandes, E.; Kennedy, S.; Chau, I.; Arrowsmith, C. H.; Schapira, M.; Vedadi, M. Kinetic characterization of human histone H3 lysine 36 methyltransferases, ASH1L and SETD2. *Biochim Biophys Acta* **2015**, 1850, 1842-8.

32. Mueller, U.; Darowski, N.; Fuchs, M. R.; Forster, R.; Hellmig, M.; Paithankar, K. S.; Puhlinger, S.; Steffien, M.; Zocher, G.; Weiss, M. S. Facilities for macromolecular crystallography at the Helmholtz-Zentrum Berlin. *Journal of Synchrotron Radiation* **2012**, 19, 442-449.

33. Kabsch, W. Xds. *Acta Crystallogr D Biol Crystallogr* **2010**, 66, 125-32.

34. Krug, M.; Weiss, M. S.; Heinemann, U.; Mueller, U. XDSAPP: a graphical user interface for the convenient processing of diffraction data using XDS. *Journal of Applied Crystallography* **2012**, 45, 568-572.

35. Emsley, P.; Lohkamp, B.; Scott, W. G.; Cowtan, K. Features and development of Coot. *Acta Crystallographica Section D-Biological Crystallography* **2010**, 66, 486-501.

36. Murshudov, G. N.; Vagin, A. A.; Dodson, E. J. Refinement of macromolecular structures by the maximum-likelihood method. *Acta Crystallographica Section D-Biological Crystallography* **1997**, 53, 240-255.

TOC graphic



SUPPORTING INFORMATION

Discovery of a potent class I PRMT fragment inhibitor

Renato Ferreira de Freitas^{1,§}, Mohammad S. Eram^{1,§}, Magdalena M. Szewczyk¹, Holger Steuber², David Smil¹, Hong Wu¹, Fengling Li¹, Guillermo Senisterra¹, Aiping Dong¹, Peter J. Brown¹, Marion Hitchcock², Dieter Moosmayer², Christian M. Stegmann², Ursula Egner², Cheryl Arrowsmith^{1,3}, Dalia Barsyte-Lovejoy¹, Masoud Vedadi^{1,4,*}, Matthieu Schapira^{1,4,*}

- p.1 Title page
- p.2 Supplementary Table 1. Selectivity profile of compound **2b**
- p.3 Supplementary Table 2. Crystallography data and refinement statistics for PRMT6 in complex with SAH and **2b** (PDB code 4QPP)
- p.4 Supplementary Figure 1. dose-dependent inhibition of PRMT1, PRMT3, CARM1, PRMT5, PRMT6, PRMT7 and PRMT8 with compounds 4 to 7
- p.5 Supplementary Table 3. Structure factors of PRMT6-fragment **7** complex structure
- p.6 Supplementary Figure 2. The superposition of the bound conformation of fragment **7** with **2** and **3**
- p.7 Supplementary Figure 3. (A) Superposition of PRMT6 in complex with fragment **3** and **7**
- p.8 Supplementary Figure 4. $F_o - F_c$ omit electron density of Fragment **7** bound to the hydrophobic exosite of PRMT6
- p.9 Supplementary Figure 5. Structural interpretation of the selectivity profile of **7**
- p.10 Supplementary Figure 6. Mechanism of action (MOA) of EPZ020411 (Compound **3**)
- p.11 Supplementary Table 4. Formula string and activity of fragment PRMT6 hits

Protein	2b	
	IC ₅₀ (μ M)	Hill slope
PRMT1	4.1	1.2
PRMT3	3.1	1.3
CARM1	0.06	0.9
PRMT5	NI	NA
PRMT6	0.07	0.8
PRMT8	1.7	0.9

Supplementary Table 1

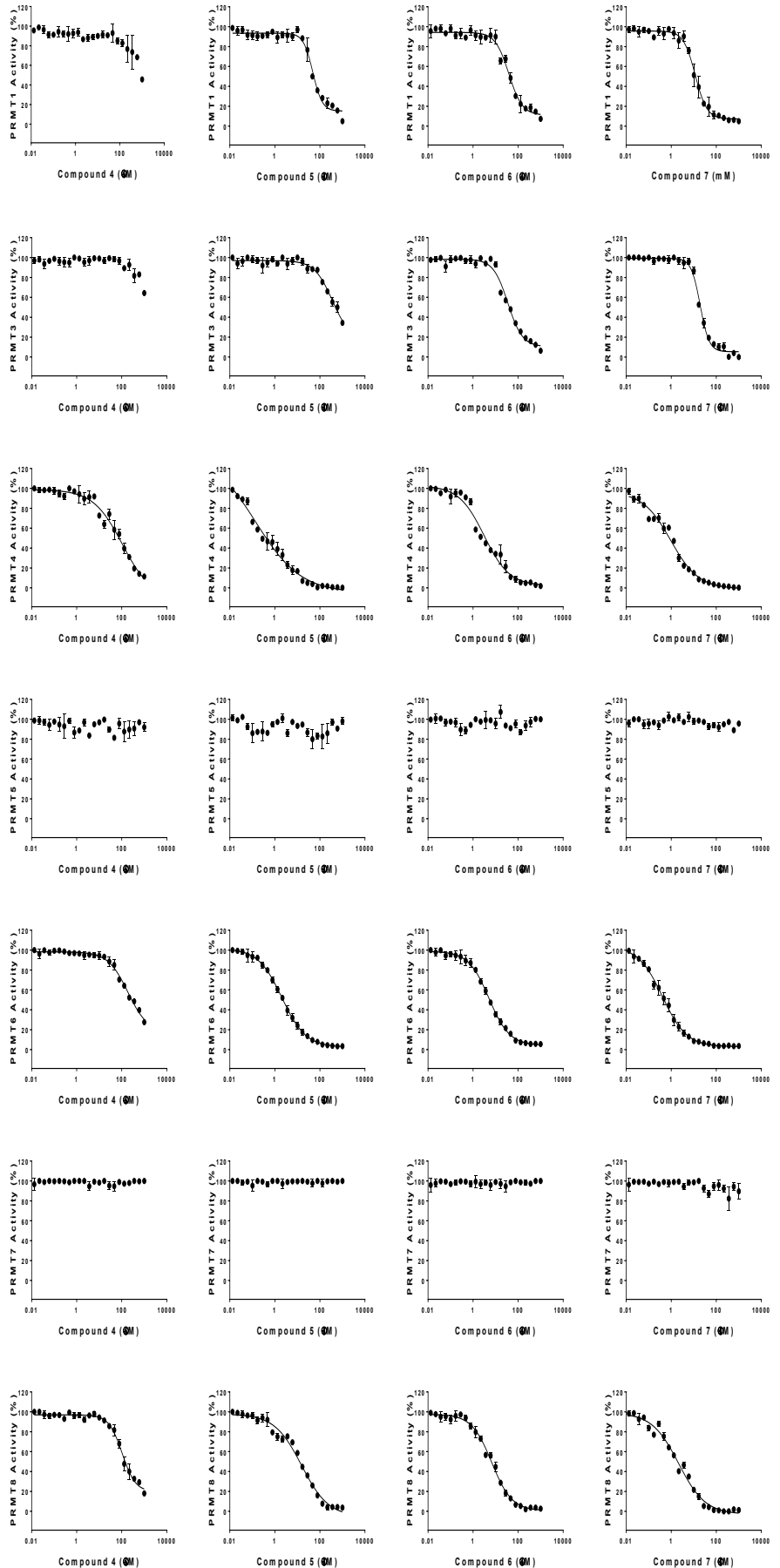
selectivity profile of compound 2b

Supplementary Table 2: Crystallography data and refinement statistics for PRMT6 in complex with SAH and **2b** (PDB code 4QPP)

PRMT6+SAH+2b	
PDB Code	4QPP
Data collection	
Space group	P4 ₂ 22
Cell dimensions	
<i>a, b, c</i> (Å)	133.9, 133.9, 133.4
α, β, γ (°)	90.0,90.0,90.0
Resolution (Å) (highest resolution shell)	50.00-2.52(2.56-2.52)
Measured reflections	336892
Unique reflections	41807
R_{merge}	13.3(90.4)
$I/\sigma I$	19.2
Completeness(%)	100.0(100.0)
Redundancy	8.2(8.1)
Refinement	
Resolution (Å)	50.0-2.52
No. reflections (test set)	41519(830)
$R_{\text{work}}/R_{\text{free}}$ (%)	23.4/19.1
No. atoms	
Protein	7708
Ligand	77
Cofactor	78
Water	291
B-factors (Å ²)	
Protein	38.1
ligand	59.7
Cofactor	36.6
Water	34.1
RMSD	
Bond lengths (Å)	0.005
Bond angles (°)	1.117
Ramachandran plot % residues	
Favored	97.2
Additional allowed	2.8
Generously allowed	0
Disallowed	0

Supplementary Figure 1

Dose-dependent
inhibition of PRMT1,
PRMT3, CARM1,
PRMT5, PRMT6,
PRMT7 and PRMT8
with compounds 4 to
7



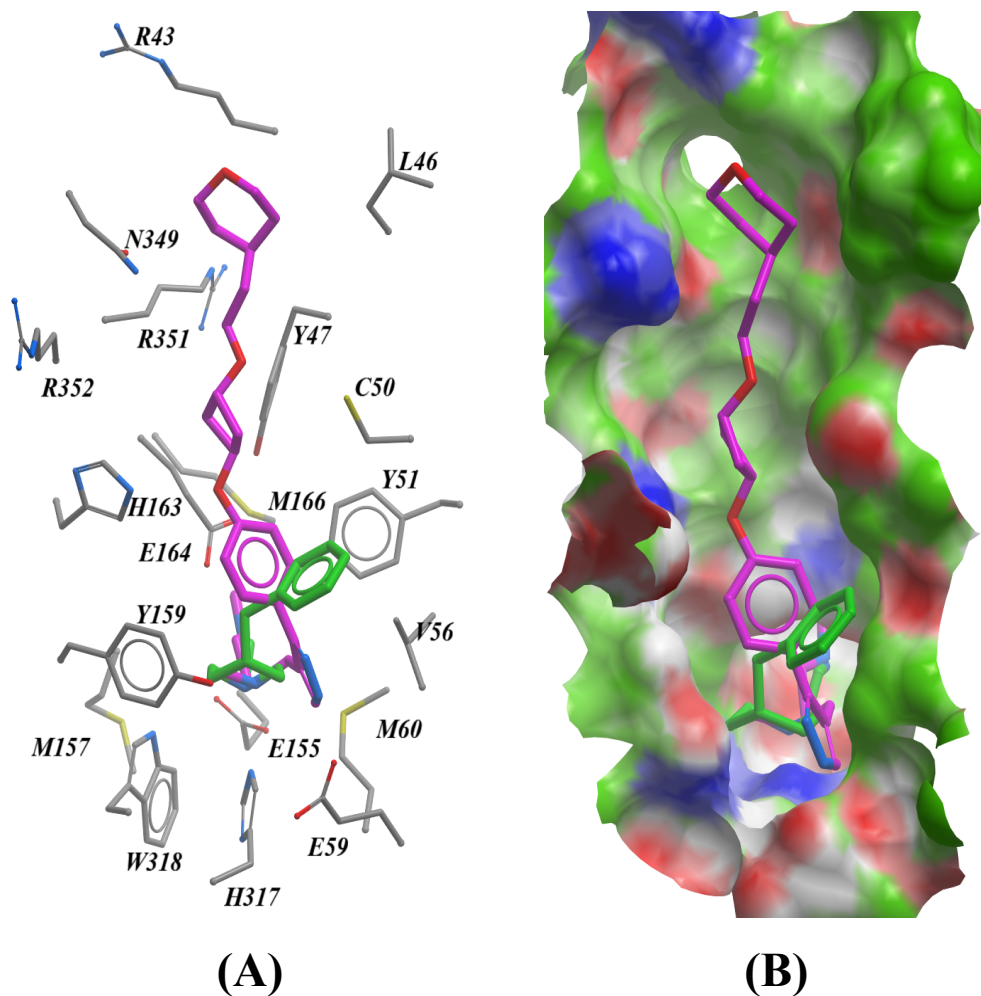
Supplementary Table 3: Structure factors of PRMT6-fragment 7 complex structure

Data Collection and Refinement Statistics: PRMT6 + SAH + 7	
PDB entry	5EGS
Data collection and Processing	
No. of crystals used	1
Wavelength [Å]	0.918409
Space group	P2 ₁
Unit cell parameters	
a, b, c [Å]	77.2; 135.6 ; 83.1
β [°]	98.91
Matthews coefficient [Å ³ /Da]	2.56
Solvent content [%]	51.9
Diffraction data	
Resolution range [Å]	50 – 2.15 (2.28-2.15)*
Unique reflections	90 370 (14 199)
$R(I)_{\text{sym}}$ [%]	14.5 (77.5)
Completeness [%]	99.2 (96.8)
Redundancy	3.8 (3.9)
$I/\sigma(I)$	8.4 (1.7)
Refinement	
Resolution range [Å]	41.26–2.15
Reflections used in refinement (work/free)	88 269 / 2 101
Final R values for all reflections (work/free) [%]	20.1 / 24.7
Protein residues	1 344
Inhibitor atoms	96 (6 molecules)
Cofactor atoms	104 (4 SAH molecules)
Water molecules	405
RMSDs	
Bonds [Å]	0.02
Angles [°]	2.1
Ramachandran plot	
Residues in most favoured regions [%]	91.3
Residues in additional allowed regions [%]	7.5
Residues in generously allowed regions [%]	0.8
Residues in disallowed regions [%]	0.4
Mean B factors [Å²]	
Protein	14.2
Inhibitor	27.2
Cofactor	21.9
Water	31.3

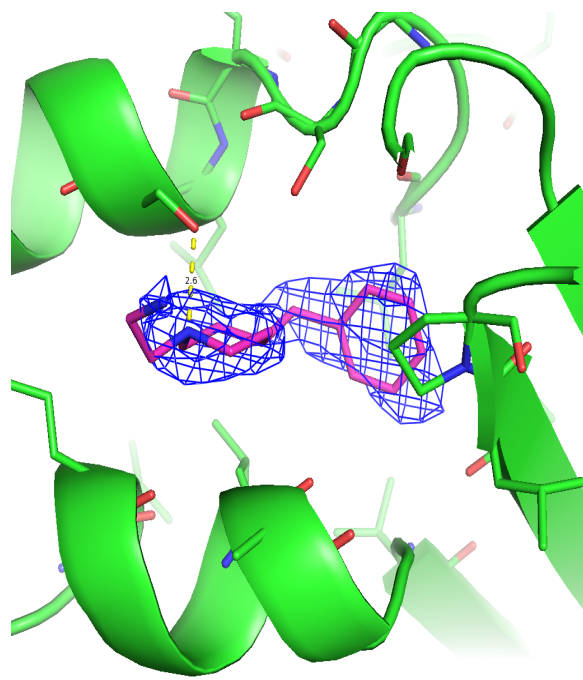
* Numbers in parentheses characterize the highest resolution shell



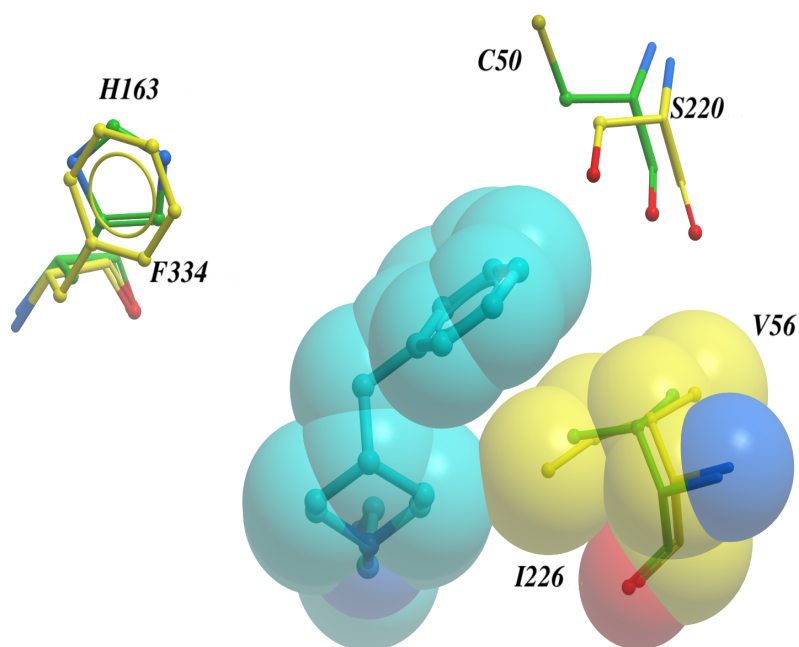
Supplementary Figure 2. The superposition of the bound conformation of fragment **7** (green) with **2** (2Y1W, yellow) and **3** (4Y30, magenta) shows that the alkylamino side chain of the inhibitors align almost perfectly. For clarity the residues of the binding pocket are hidden.



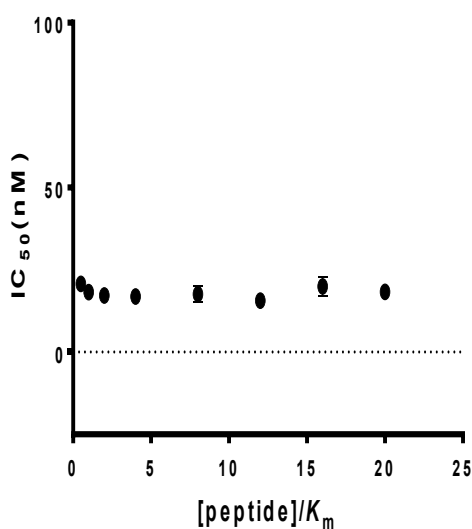
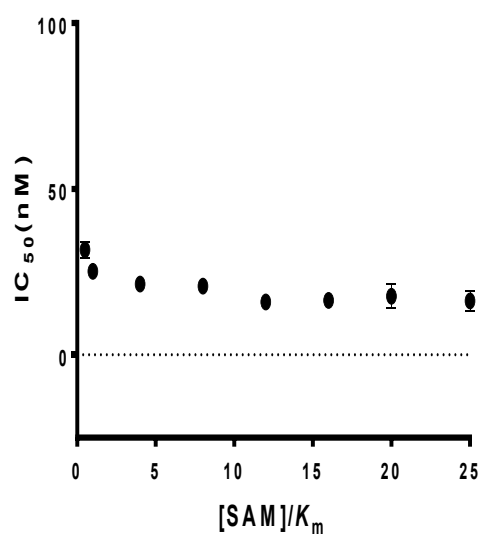
Supplementary Figure 3. (A) The superposition of the PRMT6 (green) in complex with fragment **3** (magenta) and **7** (green) shows that **3** occupies the hydrophobic shelf. For clarity, only the side chains of PRMT6-**3** are shown (colored by atom type). (B) Ligand pocket surface colored by binding properties (green, hydrophobic surface; red, hydrogen bond acceptor potential; blue, hydrogen bond donor potential).



Supplementary Figure 4. Fragment 7 (magenta) bound to the hydrophobic exosite of monomer A. The $F_o - F_c$ omit electron density is shown in blue at 2.4 s.



Supplementary Figure 5. The superposition of PRMT6 (green) in complex with fragment **7** (cyan) and PRMT3 (1F3L, yellow) indicates the possibility of a minor clash between the side chain of I226 clashes and the inhibitor. For clarity, only the residues that are different between the two enzymes are shown.

A**B**

Supplementary Figure 6. Mechanism of action (MOA) of EPZ020411 (Compound 3). MOA of compound 3 was assessed by determining IC_{50} values for the compound at varying concentrations of (A) peptide and (B) SAM at fixed concentrations of SAM (12 μ M) and peptide (2.5 μ M), respectively. The error bars represent the standard deviation of three sets of experiments.

Supplementary Table 4. Formula string and activity of fragment PRMT6 hits

Comp	SMILES	PRMT1 IC50 (μM)	PRMT3 IC50 (μM)	PRMT4 IC50 (μM)	PRMT5 IC50 (μM)	PRMT6 IC50 (μM)	PRMT7 IC50 (μM)	PRMT8 IC50 (μM)
2b	<chem>CNCCN1CCC(CC1)C1=CC=C2NC(=C(Cl)C2=C1)C1=CC=CC=C1OC</chem>	4.1	3.1	0.06	NI	0.07	ND	1.7
4	<chem>CCNC(=O)C(C)N</chem>	>1000	>1000	105 ± 7	NI	>200	NI	>200
5	<chem>CNCCN1CCC(C)CC1</chem>	48 ± 7	>500	0.2 ± 0	NI	2.1 ± 0.3	NI	15 ± 1
6	<chem>CNCCN(C)C</chem>	39 ± 3	35 ± 2	3 ± 0.2	NI	5 ± 0.6	NI	7 ± 1.2
7	<chem>NCCN1CCC(CC2=CC=CC=C2)CC1</chem>	12 ± 0.6	19 ± 1	1 ± 0.04	NI	0.3 ± 0.04	NI	2.1 ± 0.2
8	<chem>CN1CCCN(CC2=CC=C(CN)C=C2)CC1</chem>					24 ± 1		
9	<chem>NCC1=CC(CN2CCCC2)=CC=C1</chem>					360 ± 31		
10	<chem>CN(C)CC1=CC=C(CSCCN)O1</chem>					72 ± 7		
11	<chem>CNCC1=CC=CC(=C1)C1=CSC=C1</chem>					69 ± 5		
12	<chem>CNCC1=CC=C(C)S1</chem>					99 ± 6		
13	<chem>CNCC1=CC=CC(=C1)C1=CC=NC=C1</chem>					100 ± 18		
14	<chem>CNCC1=CC(=CC=C1)C1=CC=CS1</chem>					125 ± 23		
15	<chem>CNCC1=CC=CC(=C1)C1=CC=CN=C1</chem>					104 ± 9		
16	<chem>CC1=C(SC(N)=N1)N1C=CC(=N1)C(F)(F)F</chem>					46 ± 5		
17	<chem>CNCC1=CC(=CC=C1)C1=CSC(C)=N1</chem>					136 ± 24		
18	<chem>CNCC1=CC(=CC=C1)C1=CC=CO1</chem>					146 ± 13		
19	<chem>NC1=CC=C(C=C1)S(=O)(=O)NC1=NC=CS1</chem>					430 ± 34		
20	<chem>CNCC1=CC=CC(=C1)N1CCCC1</chem>					170 ± 8		